YAP/TAZ mediate TGFβ2-induced Schlemm's canal cell dysfunction

Haiyan Li[a,b,c], Kristin M. Perkumas[d], W. Daniel Stamer[d,e], Preethi S. Ganapathy[a,c,f,], Samuel Herberg[a,b,c,g,h*]

Affiliations:

[a] Department of Ophthalmology and Visual Sciences, SUNY Upstate Medical University, Syracuse, NY 13210, USA

[b] Department of Cell and Developmental Biology, SUNY Upstate Medical University, Syracuse, NY 13210, USA

[c] BioInspired Institute, Syracuse University, Syracuse, NY 13244, USA

[d] Department of Ophthalmology, Duke Eye Center, Duke University, Durham, NC 27708, USA

[e] Department of Biomedical Engineering, Duke University, Durham, NC 27708, USA

[f] Department of Neuroscience and Physiology, SUNY Upstate Medical University, Syracuse, NY 13210, USA

[g] Department of Biochemistry and Molecular Biology, SUNY Upstate Medical University, Syracuse, NY 13210, USA

[h] Department of Biomedical and Chemical Engineering, Syracuse University, Syracuse, NY 13244, USA

*To whom correspondence should be addressed: Samuel Herberg, PhD, Assistant Professor; Department of Ophthalmology and Visual Sciences, SUNY Upstate Medical University, 505 Irving Avenue, Neuroscience Research Building Room 4609, Syracuse, NY 13210, USA, email: herbergs@upstate.edu

Keywords: POAG, mechanotransduction, TM stiffness, hydrogel, actin cytoskeleton

Abstract

Purpose: Elevated transforming growth factor beta2 (TGFβ2) levels in the aqueous humor have been linked to glaucomatous outflow tissue dysfunction. Potential mediators of dysfunction are the transcriptional co-activators, Yes-associated protein (YAP) and transcriptional coactivator with PDZ binding motif (TAZ). However, the molecular underpinnings of YAP/TAZ modulation in SC cells under glaucomatous conditions are not well understood. Here, we investigate how TGFβ2 regulates YAP/TAZ activity in human SC (HSC) cells using biomimetic extracellular matrix (ECM) hydrogels, and examine whether pharmacologic YAP/TAZ inhibition would attenuate TGFβ2-induced HSC cell dysfunction.

Methods: Primary HSC cells were seeded atop photocrosslinked ECM hydrogels, made of collagen type I, elastin-like polypeptide and hyaluronic acid, or encapsulated within the hydrogels. Changes in actin cytoskeleton, YAP/TAZ activity, ECM production, phospho-myosin light chain levels, and hydrogel contraction were assessed.

Results: TGFβ2 significantly increased YAP/TAZ nuclear localization in HSC cells, which was prevented by either filamentous (F)-actin relaxation or depolymerization. Pharmacologic YAP/TAZ inhibition using verteporfin decreased fibronectin expression and reduced actomyosin cytoskeletal rearrangement in HSC cells induced by TGFβ2. Similarly, verteporfin significantly attenuated TGFβ2-induced HSC cell-encapsulated hydrogel contraction.

Conclusions: Our data provide evidence for a pathologic role of aberrant YAP/TAZ signaling in HSC cells under simulated glaucomatous conditions, and suggest that pharmacologic YAP/TAZ inhibition has promising potential to improve outflow tissue dysfunction.

51 **Introduction**

52 The Schlemm's canal (SC) is a continuous vessel that encircles the anterior chamber at the
53 iridocorneal angle; its lumen is lined with a single non-fenestrated layer of endothelial cells having
54 both blood and lymphatic characteristics [1-5]. Situated in close apposition to the trabecular
55 meshwork (TM), the SC is divided into the inner and outer wall [2]. The SC inner wall experiences
56 a basal-to-apical pressure gradient (intraocular versus episcleral venous pressures) that drives
57 aqueous humor into the SC lumen, which is then drained into the collector channels and aqueous
58 veins [6]. Most of the resistance to aqueous humor outflow is generated at, or close to the SC inner
59 wall in a region called the juxtacanalicular tissue (JCT) of the TM [7-9]. Importantly, increased
60 outflow resistance in the JCT leads to elevated intraocular pressure (IOP), the only modifiable risk
61 factor for primary open-angle glaucoma (POAG) [8, 10-13].

62 Previous studies have demonstrated that glaucomatous SC cells isolated from POAG eyes
63 exhibited higher levels of filamentous (F)-actin, α-smooth muscle actin (αSMA) and fibronectin,
64 as well as increased cell stiffness compared to normal SC cells [14, 15]. The ocular hypertension-
65 causing steroid dexamethasone was shown to increase F-actin fibers, while the IOP-lowering Rho-
66 associated kinase (ROCK) inhibitor Y27632 decreased F-actin levels [16, 17]; F-actin is thought to
67 mediate SC cell contractility and stiffness to negatively affect aqueous humor outflow and IOP [18].
68 Thus, SC cell dysfunction is thought to be a significant contributor to the increased outflow
69 resistance in POAG; however, the mechanistic underpinnings of SC cell pathobiology remain
70 incompletely understood.

71 Transforming growth factor beta 2 (TGFβ2), the predominant TGFβ isoform in the eye and
72 aqueous humor, is a major player in contributing to the pathologic changes in POAG [10, 19-23]. It has
73 been shown that levels of TGFβ2 are elevated in eyes of glaucoma patients compared to age-

74 matched normal eyes [21, 22, 24, 25]. In culture, TM and SC cells isolated from donor eyes with POAG
75 secrete more active TGFβ2 protein compared to normal cells [15, 26]. Accordingly, perfusion of
76 TGFβ2 in human anterior segments increases resistance in the conventional outflow pathway [27].
77 At the cellular level, TGFβ2 increases actin stress fibers and phospho-myosin light chain (p-MLC)
78 to drive pathologic TM cell contraction [28-30]. Moreover, exposure of TM cells to TGFβ2 induces
79 the expression/deposition of extracellular matrix (ECM) proteins such as collagen types I and IV,
80 and fibronectin [28, 31-33]. Despite the progress made in uncovering the role of TGFβ2 in TM cell
81 dysfunction, the contributions of TGFβ2 to SC cell pathobiology are less well understood.

82 Yes-associated protein (YAP) and transcriptional coactivator with PDZ-binding motif (TAZ)
83 are powerful regulators of cell proliferation and differentiation, with an established link to tissue
84 fibrosis [34-38]. Upon nuclear translocation, YAP/TAZ interact with TEA domain (TEAD)
85 transcription factors to drive the expression of known (CTGF, CYR61, ANKRD1) and glaucoma-
86 related putative downstream effectors of active YAP/TAZ signaling (e.g., transglutaminase-2
87 (TGM2)) [39]. To that end, *YAP1* was recently identified among a group of previously unknown
88 POAG risk loci across European, Asian and African ancestries, suggesting a potential causal
89 association with outflow dysfunction [40]. YAP/TAZ can be activated by multiple stimuli, such as
90 stiffened ECM, increased mechanical stress, and exposure to growth factors [41, 42]. Recently, we
91 demonstrated that both ECM stiffening and TGFβ2 increase YAP/TAZ activity in human TM cells,
92 which was linked to pathologic cell contractility and ECM remodeling that may exacerbate
93 glaucoma pathology [26].

94 The physiological substrate of the SC inner wall endothelial cells is its discontinuous basal
95 lamina, which is in direct contact with the JCT [3, 6]. Recently, we developed a bioengineered
96 hydrogel composed of ECM biopolymers found in the native JCT region encapsulated with human

97 TM (HTM) cells, and demonstrated its utility for studying cell-ECM interactions under normal
98 and simulated glaucomatous conditions in a relevant tissue-mimetic 3D microenvironment [26, 30, 43].
99 Here, we investigated the effects of TGFβ2 on regulating YAP/TAZ activity in human SC (HSC)
100 cells cultured atop the acellular ECM hydrogel. Additionally, we examined whether
101 pharmacologic YAP/TAZ inhibition would alleviate TGFβ2-induced HSC cell dysfunction.
102

103 **Materials and Methods**

104 ***HSC cell isolation and culture***

105 Experiments using human donor eye tissue were approved by the SUNY Upstate Medical
106 University Institutional Review Board (protocol #1211036), and were performed in accordance
107 with the tenets of the Declaration of Helsinki for the use of human tissue. Primary HSC cells were
108 isolated from healthy donor corneal rims discarded after transplant surgery and cultured according
109 to established protocols [5]. Briefly, the corneal rims were cut into wedges and placed into a 100
110 mm dish containing low-glucose Dulbecco's Modified Eagle's Medium (DMEM; Gibco; Thermo
111 Fisher Scientific, Waltham, MA, USA) with 10% fetal bovine serum (FBS; Atlanta Biologicals,
112 Flowery Branch, GA, USA) and 1% penicillin/streptomycin/glutamine (PSG; Gibco). Using an
113 SMZ1270 stereomicroscope (Nikon Instruments, Melville, NY, USA), a 2% gelatin-coated
114 (Sigma-Aldrich) 6-0 nylon monofilament sterile suture (eSutures, Mokena, IL, USA) was inserted
115 into the SC lumen of each wedge with fine-tipped forceps (Fine Science Tools, Foster City, CA,
116 USA), and these wedges were cultured in DMEM with 10% FBS and 1% PSG, and maintained at
117 37°C in a humidified atmosphere with 5% CO_2 for 3 weeks. Next, curvilinear incisions were made
118 parallel to Schwalbe's line (alongside the suture) into the TM, which produced a TM flap. After
119 lifting the TM, the sutures were gently removed, and a ~2 mm long piece was cut from each end

120 of the suture to prevent fibrotic cell contamination. Next, the sutures were washed with Dulbecco's
121 Phosphate Buffered Saline (DPBS; Gibco), placed into a single well of gelatin-coated (Sigma-
122 Aldrich) 6-well culture plates (Corning; Thermo Fisher Scientific), and digested for 2 min with
123 0.25% trypsin/0.5 mM EDTA (Gibco). Subsequently, 5 ml DMEM with 10% FBS and 1% PSG
124 were added, and the sutures were moved to another gelatin-coated well. The digests and sutures
125 were cultured in DMEM with 10% FBS and 1% PSG, and maintained at 37°C in a humidified
126 atmosphere with 5% CO_2. Fresh media was supplied every 2-3 days. Once confluent, HSC cells
127 were lifted with 0.25% trypsin/0.5 mM EDTA and sub-cultured in DMEM with 10% FBS and 1%
128 PSG. All studies were conducted using cells passage 3-6. Four HSC cell strains (HSC01, HSC02,
129 HSC03, HSC09) were characterized and used for the experiments herein; the reference cell strain
130 HSC78 was isolated and characterized at Duke University by K.M.P. and W.D.S. (**Table 1**).
131 Different combinations of 2-3 HSC cell strains were used per experiment, depending on cell
132 availability.

133

134 **Table 1: HSC cell strain information.**

ID	Sex	Age
HSC01	Male	33
HSC02	Male	46
HSC03	Female	46
HSC09	Female	69
Reference HSC78*	Male	77
**obtained from W.D.S. at Duke University*		

135

136

137 ***HSC cell characterization***

138 HSC cells were seeded at 1×10^4 cells/cm^2 in 6-well culture plates or on sterilized glass
139 coverslips in 24-well culture plates, and cultured in DMEM with 10% FBS and 1% PSG. HSC cell
140 morphology and growth characteristics were monitored by phase contrast microscopy using an
141 LMI-3000 Series Routine Inverted Microscope (Laxco; Thermo Fisher Scientific). Once confluent,
142 monolayers of HSC cells were processed for immunocytochemistry and immunoblot analyses to
143 assess expression of fibulin-2 and vascular endothelial-cadherin (VE-CAD), respectively. To rule
144 out the contamination of HTM cells, dexamethasone (DEX; Fisher Scientific)-induced myocilin
145 (MYOC) expression was assessed in HSC cells. Briefly, confluent HSC cells were treated with
146 100 nM DEX or vehicle control (0.1% (v/v) ethanol) in DMEM with 1% FBS and 1% PSG for 4
147 d, and serum- and phenol red-free DMEM for 3 d. The HSC cell culture supernatants were
148 collected and concentrated using Amicon® Ultra Centrifugal Filters (Millipore Sigma, Burlington,
149 MA, USA) for immunoblot analysis.

150

151 ***Preparation of ECM thin-film hydrogels***

152 Hydrogel precursors methacrylate-conjugated bovine collagen type I (MA-COL, Advanced
153 BioMatrix, Carlsbad, CA, USA; 3.6 mg/ml [all final concentrations]), thiol-conjugated hyaluronic
154 acid (SH-HA, Glycosil®, Advanced BioMatrix; 0.5 mg/ml, 0.025% (w/v) photoinitiator Irgacure®
155 2959; Sigma-Aldrich, St. Louis, MO, USA) and in-house expressed elastin-like polypeptide (SH-
156 ELP, thiol via K<u>C</u>TS flanks [43]; 2.5 mg/ml) were thoroughly mixed. Thirty microliters of the
157 hydrogel solution were pipetted onto a Surfasil (Fisher Scientific)-coated 18 × 18-mm square glass
158 coverslip followed by placing a regular 12-mm round glass coverslip onto the hydrogels.
159 Constructs were crosslinked by exposure to UV light (OmniCure S1500 UV Spot Curing System;

160 Excelitas Technologies, Mississauga, Ontario, Canada) at 320-500 nm, 2.2 W/cm^2 for 5 s, as
161 previously described [26, 30, 43]. The hydrogel-adhered coverslips were removed with fine-tipped
162 tweezers and placed in 24-well culture plates (Corning; Thermo Fisher Scientific).
163
164 ***HSC cell treatments***

165 HSC cells were seeded at 2 × 10^4 cells/cm^2 atop premade ECM hydrogels and cultured in
166 DMEM with 10% FBS and 1% PSG for 1 or 2 days. Then, HSC cells were cultured in serum-free
167 DMEM with 1% PSG and subjected to the different treatments for 3 d: TGFβ2 (2.5 ng/ml; R&D
168 Systems, Minneapolis, MN, USA), the ROCK inhibitor Y27632 (10 μM; Sigma-Aldrich), the actin
169 depolymerizer latrunculin B (10 μM; for 30 min only to preserve cell viability; Tocris Bioscience;
170 Thermo Fisher Scientific), or the YAP inhibitor verteporfin (0.5 μM; Sigma).
171
172 ***Immunoblot analysis***

173 Equal protein amounts (10 μg), determined by standard bicinchoninic acid assay (Pierce;
174 Thermo Fisher Scientific), from HSC cell lysates in lysis buffer (CelLytic™ M, Sigma-Aldrich)
175 or from concentrated HSC cell culture supernatants ± DEX at 7 d supplemented with Halt™
176 protease/phosphatase inhibitor cocktail (Thermo Fisher Scientific) in 4× loading buffer (Invitrogen;
177 Thermo Fisher Scientific) with 5% beta-mercaptoethanol (Fisher Scientific) were boiled for 5 min,
178 subjected to SDS-PAGE using NuPAGE™ 4-12% Bis-Tris Gels (Invitrogen; Thermo Fisher
179 Scientific) at 120V for 80 min, and transferred to 0.45 μm PVDF membranes (Sigma; Thermo
180 Fisher Scientific). Membranes were blocked with 5% bovine serum albumin (Thermo Fisher
181 Scientific) in tris-buffered saline with 0.2% Tween®20 (Thermo Fisher Scientific), and probed
182 with various primary antibodies followed by incubation with HRP-conjugated secondary

183 antibodies or fluorescent secondary antibodies (LI-COR, Lincoln, NE, USA). Bound antibodies
184 were visualized with the enhanced chemiluminescent detection system (Pierce) on
185 autoradiography film (Thermo Fisher Scientific) or Odyssey® CLx imager (LI-COR). A list of all
186 antibodies and their working dilutions can be found in **Supplementary Table 1**.
187
188 ***Immunocytochemistry analysis***
189 HSC cells atop ECM hydrogels subjected to the different treatments for 3 d were fixed with 4%
190 paraformaldehyde (Thermo Fisher Scientific) at room temperature for 20 min, permeabilized with
191 0.5% Triton™ X-100 (Thermo Fisher Scientific), blocked with blocking buffer (BioGeneX), and
192 incubated with primary antibodies, followed by incubation with fluorescent secondary antibodies;
193 nuclei were counterstained with 4′,6′-diamidino-2-phenylindole (DAPI; Abcam). Similarly, cells
194 were stained with Phalloidin-iFluor 488 (Invitrogen) or 594 (Abcam)/DAPI according to the
195 manufacturer's instructions. Coverslips were mounted with ProLong™ Gold Antifade (Invitrogen)
196 on Superfrost™ microscope slides (Fisher Scientific), and fluorescent images were acquired with
197 an Eclipse N*i* microscope (Nikon Instruments, Melville, NY, USA). A list of all antibodies and
198 their working dilutions can be found in **Supplementary Table 1**.
199
200 ***Image analysis***
201 All image analyses were performed using FIJI software (National Institutes of Health (NIH),
202 Bethesda, MD, USA). Briefly, the cytoplasmic YAP/TAZ intensity was measured by subtracting
203 the overlapping nuclear (DAPI) intensity from the total YAP/TAZ intensity. The nuclear
204 YAP/TAZ intensity was recorded as the proportion of total YAP/TAZ intensity that overlapped
205 with the nucleus (DAPI). YAP/TAZ nuclear/cytoplasmic (N/C) ratio was calculated as follows:

206 N/C ratio = (nuclear YAP/TAZ signal/area of nucleus)/(cytoplasmic signal/area of cytoplasm).
207 Fluorescence intensity of F-actin, FN, TGM2, and p-MLC were measured in at least 30 images
208 from 3 HSC cell strains with 3 replicates per HSC cell strain with image background subtraction
209 using FIJI software. Given the lack of defined αSMA fibers in untreated controls, we measured
210 the percent of αSMA-positive cells using FIJI software. At least 150 cells were analyzed in 30
211 images from 3 HSC cell strains with 3 replicates per HSC cell strain.
212
213 ***HSC hydrogel contraction analysis.***
214 HSC cell-laden hydrogels were prepared by mixing HSC cells (1.0×10^6 cells/ml) with MA-
215 COL (3.6 mg/ml), SH-HA (0.5 mg/ml, 0.025% (w/v) photoinitiator) and SH-ELP (2.5 mg/ml) on
216 ice, followed by pipetting 10 µl droplets of the HSC cell-laden hydrogel precursor solution onto
217 polydimethylsiloxane (PDMS; Sylgard 184; Dow Corning)-coated 24-well culture plates.
218 Constructs were crosslinked as described above (320-500 nm, 2.2 W/cm^2, 5 s). HSC cell-laden
219 hydrogels were cultured in DMEM with 10% FBS and 1% PSG in presence of the different
220 treatments. Longitudinal brightfield images were acquired at 0 d and 5 d with an Eclipse T*i*
221 microscope (Nikon). Construct area from N = 12 hydrogels per group from 3 HSC cell strains with
222 4 replicates per cell strain was measured using FIJI software and normalized to 0 d followed by
223 normalization to controls.
224
225 ***HSC hydrogel cell viability analysis***
226 Cell viability was measured with the CellTiter 96® Aqueous Non-Radioactive Cell
227 Proliferation Assay (Promega) following the manufacturer's protocol. HSC hydrogels cultured in
228 DMEM with 10% FBS and 1% PSG in presence of the different treatments for 5 d were incubated

229 with the staining solution (38 µl MTS, 2 µl PMS solution, 200 µl DMEM) at 37ºC for 1.5 h.
230 Absorbance at 490 nm was recorded using a spectrophotometer plate reader (BioTek, Winooski,
231 VT, USA). Blank-subtracted absorbance values served as a direct measure of HSC cell viability
232 from N = 12 hydrogels per group from 3 HSC cell strains with 4 replicates per cell strain.

233

234 ***Statistical analysis***

235 Individual sample sizes are specified in each figure caption. Comparisons between groups were
236 assessed by two-way analysis of variance (ANOVA) with Tukey's multiple comparisons *post hoc*
237 tests, as appropriate. The significance level was set at $p<0.05$ or lower. GraphPad Prism software
238 v9.2 (GraphPad Software, La Jolla, CA, USA) was used for all analyses.

239

240 **Results**

241 ***HSC cell characterization***

242 Four HSC cell strains (HSC01, HSC02, HSC03, and HSC09) were used and compared to a
243 validated reference strain (HSC78). All of our HSC cell strains exhibited typical spindle-like
244 elongated cell morphology comparable to the reference standard (**Fig. 1A**). A reliable feature of
245 HSC cells *in vitro* is expression of two positive markers, fibulin-2 and vascular endothelial-
246 cadherin (VE-CAD) [44]. Our results show that all HSC cell strains highly expressed fibulin-2 (**Fig.**
247 **1B**) and VE-CAD (**Fig. 1C**), comparable to the reference strain. In culture, HTM cells upregulate
248 MYOC expression following challenge with the corticosteroid DEX [45], whereas this does not occur
249 in HSC cells. We observed that none of the HSC cell strains expressed MYOC in response to DEX
250 treatment (**Fig. 1D**), suggesting pure HSC cell preparations devoid of HTM cell contamination.

Together, these data suggest that HSC01, HSC02, HSC03, and HSC09 exhibit required key characteristics according to previous publications [5, 44] to faithfully identify them as normal HSC cells, comparable to a confirmed reference standard.

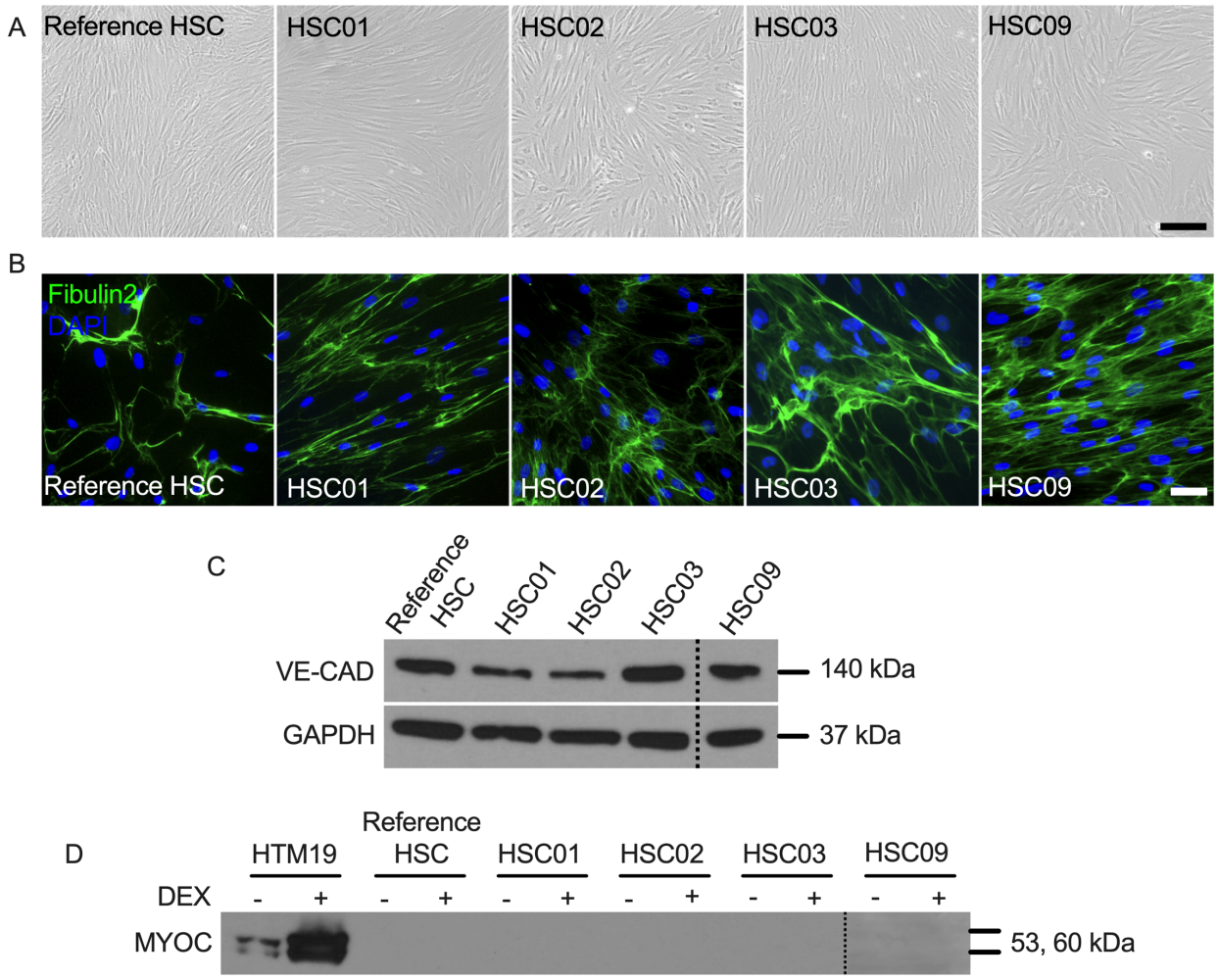

Fig. 1. HSC cell characterization. (A) Representative phase contrast micrographs of reference HSC, HSC01, HSC02, HSC03, and HSC09 cell strains. Scale bar, 200 µm. (B) Representative immunofluorescence micrographs of fibulin-2. Scale bar, 100 µm. (C) Immunoblot of VE-Cadherin (VE-CAD). (D) Immunoblot of secreted myocilin (MYOC) at 7 d (= negative marker).

260 ***Effects of TGFβ2 in the absence or presence of ROCK inhibition or Lat B on actin cytoskeleton***
261 ***in HSC cells.***

262 F-actin levels are higher in SC cells isolated from POAG eyes compared to normal SC cells [15].
263 To investigate the effects of TGFβ2 on actin cytoskeleton remodeling, HSC cells were cultured
264 atop premade ECM hydrogels and treated with TGFβ2 alone, or co-treated with ROCK inhibitor
265 Y27632 or latrunculin B (Lat B), a compound that inhibits actin polymerization (**Fig. 2A**). We
266 observed significantly increased F-actin fibers in HSC cells treated with TGFβ2 compared to
267 controls, which was significantly prevented by co-treatment with Y27632 or Lat B co-treatment;
268 with acute Lat B treatment showing a stronger effect (**Fig. 2B,C**). Of note, both types of actin
269 destabilizers failed to fully block TGFβ2-induced F-actin assembly. We observed a range of
270 responsiveness to the TGFβ2 challenge ± treatments among the HSC cell strains, indicating normal
271 donor-to-donor viability.

272 We, and others, have shown that the fibrotic marker α-smooth muscle actin (αSMA) is
273 upregulated in HTM cells by TGFβ2 exposure [28-30, 46]. Here, we demonstrated that TGFβ2 induced
274 expression of αSMA in 45.87% of HSC cells compared to only ~3.16% in controls. Similar to
275 results with F-actin, Y27632 prevented αSMA expression induced by TGFβ2, with only 13.98%
276 αSMA^+ cells. Interestingly, short term Lat B treatment failed to block TGFβ2-induced αSMA
277 expression (% of αSMA^+ cells: 41.95%) (**Fig. 2D,E**).

278 Collectively, these data demonstrate that TGFβ2 upregulates F-actin fibers in HSC cells, which
279 is decreased by either actin cytoskeleton relaxation or depolymerization. Furthermore, TGFβ2
280 induces αSMA expression, which is prevented by ROCK inhibition, whereas short-term actin
281 depolymerization does not influence aberrant αSMA stress fiber formation independent on the cell
282 strain used.

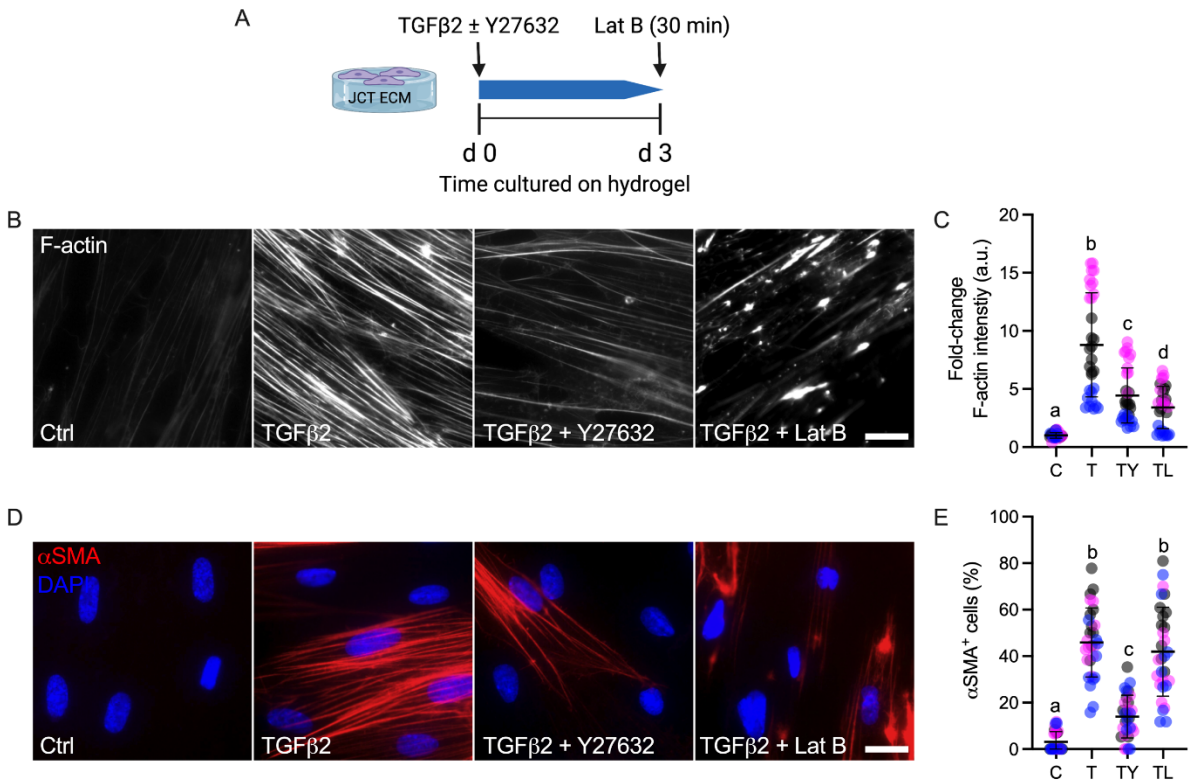

Fig. 2. Effects of TGFβ2 in the absence or presence of a ROCK inhibitor or Lat B on F-actin and αSMA stress fibers in HSC cells. (A) Schematic showing time course of the different treatments. (B) Representative fluorescence micrographs of F-actin in HSC cells on ECM hydrogel substrates subjected to control, TGFβ2 (3 d; 2.5 ng/mL), TGFβ2 + Y27632 (3 d; 10 μM), TGFβ2 (3 d) + Lat B (30 min; 2 μM). Scale bar, 20 μm. (C) Analysis of F-actin intensity (N = 30 images per group from 3 HSC cell strains with 3 replicates per HSC cell strain). (D) Representative immunofluorescence micrographs of αSMA in HSC cells on ECM hydrogel substrates subjected to the different treatments. Scale bar, 20 μm. (E) Analysis of percentage of αSMA^{+} cells (N = 30 images per group from 3 HSC cell strains with 3 experimental replicates per HSC cell strain; more than 150 cells were analyzed per cell strain). Symbols with different colors represent different cell strains. The bars and error bars indicate Mean ± SD. Significance was determined by two-way ANOVA using multiple comparisons tests (shared significance indicator letters represent non-significant difference ($p>0.05$), distinct letters represent significant difference ($p<0.05$)).

299 ***TGFβ2 stabilizes actin cytoskeleton to upregulate YAP/TAZ activity***

300 Recently, we demonstrated that TGFβ2 increases nuclear YAP and TAZ, a readout for active
301 YAP/TAZ signaling, in HTM cells cultured atop or within ECM hydrogels [26]. To assess the effect
302 of TGFβ2 on YAP/TAZ subcellular localization in HSC cells subjected to the different treatments,
303 we evaluated both YAP and TAZ nuclear-to-cytoplasmic (N/C) ratios. We observed that exposure
304 to TGFβ2 significantly increased YAP N/C ratio (**Fig. 3A,B**), TAZ N/C ratio (**Fig. 3C,D**), and
305 expression of their putative downstream effector TGM2 (**Fig. 3E,F**) compared to controls;
306 suggesting that TGFβ2 enhanced YAP/TAZ transcriptional activity. Given that actin cytoskeletal
307 integrity is required for proper YAP/TAZ regulation in a variety of cells [41, 47], we investigated
308 whether TGFβ2-induced YAP/TAZ activation in HSC cells depended on an intact actin
309 cytoskeleton. Our results revealed that HSC cells co-treated with Y27632 or Lat B significantly
310 decreased TGFβ2-induced YAP/TAZ nuclear localization and TGM2 expression. Consistent with
311 our observation on F-actin fibers in response to the different treatments, Lat B was more effective
312 in decreasing YAP/TAZ activity in HSC cells (i.e., below control levels) compared to Y27632
313 (**Fig. 3A-F**).

314 Together, these data show that TGFβ2 increases nuclear YAP/TAZ and TGM2 expression in
315 HSC cells from multiple donors, which is potently attenuated by either actin cytoskeleton
316 relaxation or depolymerization.

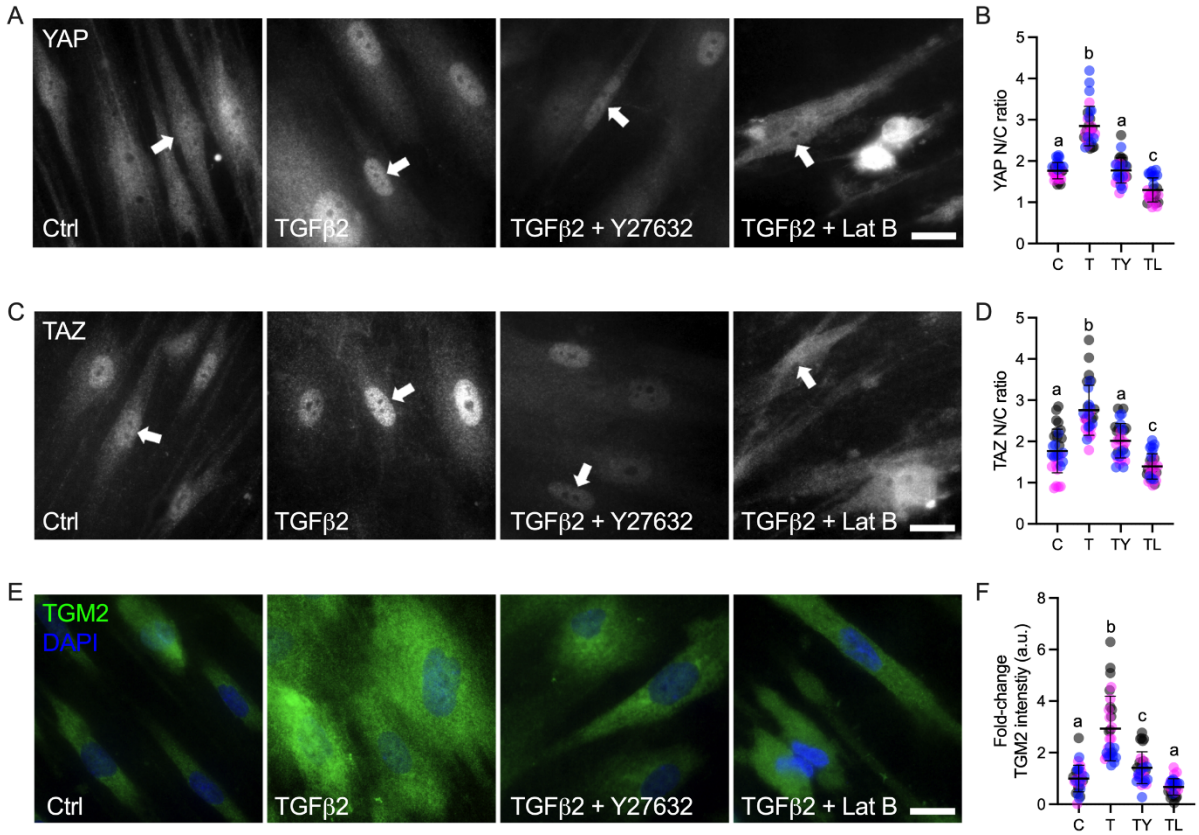

Fig. 3. Effects of TGFβ2 in the absence or presence of a ROCK inhibitor or Lat B on YAP/TAZ activity in HSC cells. (A and B) Representative immunofluorescence micrographs of YAP and TAZ in HSC cells on ECM hydrogel substrates subjected to control, TGFβ2 (3 d; 2.5 ng/mL), TGFβ2 + Y27632 (3 d; 10 μM), TGFβ2 (3 d) + Lat B (30 min; 2 μM). Scale bar, 20 μm; arrows indicate YAP/TAZ nuclear localization. (C and D) Analysis of YAP/TAZ nuclear/cytoplasmic ratio (N = 30 images from 3 HSC cell strains with 3 experimental replicates per cell strain). (E) Representative fluorescence micrographs of TGM2 in HSC cells on ECM hydrogel substrates subjected to the different treatments. Scale bar, 20 μm. (F) Analysis of TGM2 intensity (N = 30 images from 3 HSC cell strains with 3 replicates per cell strain). Symbols with different colors represent different cell strains. The bars and error bars indicate Mean ± SD. Significance was determined by two-way ANOVA using multiple comparisons tests (shared significance indicator letters represent non-significant difference ($p>0.05$), distinct letters represent significant difference ($p<0.05$)).

YAP/TAZ mediate ECM remodeling and actomyosin cell cytoskeleton

It has been shown that HSC cells isolated from glaucomatous eyes exhibit increased F-actin levels and expression of ECM proteins including fibronectin [15]; in this study, our results suggest that TGFβ2 also increases actin cytoskeleton remodeling. Both abnormal ECM deposition and

336 actin remodeling may be part of a pathologic signature in HSC cells. Therefore, we next tested
337 whether pharmacologic YAP/TAZ inhibition could rescue TGFβ2-induced HSC cell dysfunction.
338 To do so, HSC cells atop ECM hydrogels were treated with TGFβ2 alone or co-treated with
339 verteporfin (VP), which disrupts nuclear YAP/TAZ-TEAD interactions thereby inhibiting
340 transcriptional activity [48]. Co-treatment of VP with TGFβ2 significantly decreased N/C ratios of
341 YAP and TAZ in HSC cells compared to TGFβ2 alone, approximating baseline levels (**Suppl. Fig.**
342 **1A-D**). Similarly, VP significantly decreased TGFβ2-stimulated TGM2 expression; yet, levels
343 remained significantly higher compared to controls (**Suppl. Fig. 1E,F**).

344 We observed that exposure to VP significantly reduced TGFβ2-induced fibronectin deposition
345 approximating untreated controls (**Fig. 4A,B**). Importantly, we demonstrated that TGFβ2-induced
346 αSMA expression (**Fig. 4C,D**), F-actin fibers (**Fig. 4E,F**), and phospho-myosin light chain (p-
347 MLC) levels (**Fig. 4G,H**) were significantly decreased by VP co-treatment, but again did not reach
348 baseline levels.

349 In sum, these data suggest that pharmacologic YAP/TAZ inhibition reduces the expression of
350 fibronectin and decreases actomyosin cytoskeletal rearrangement independent of the cell strain
351 used.

352

353

354

355

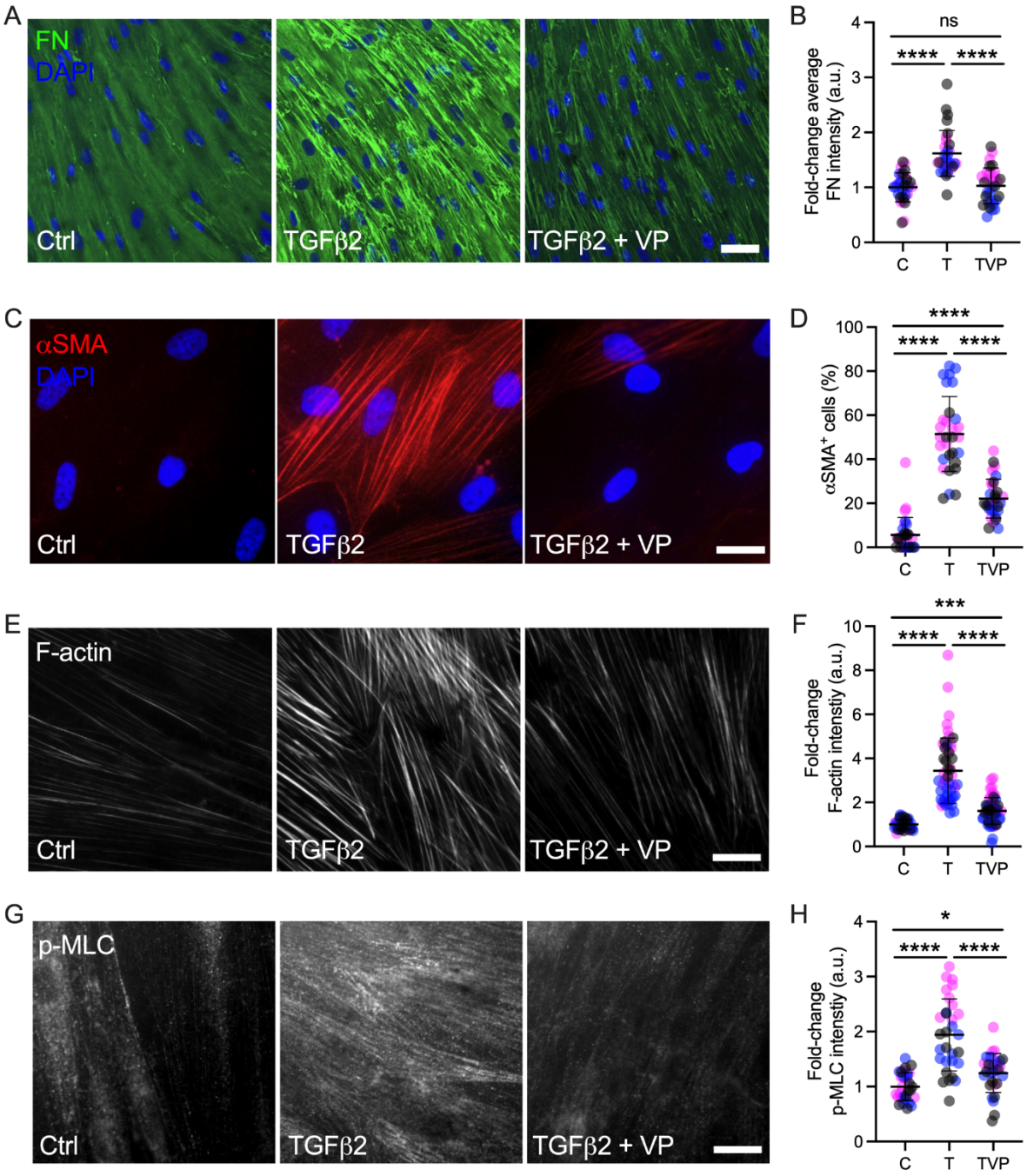

Fig. 4. Effects of YAP/TAZ inhibition on ECM remodeling and actomyosin cytoskeleton in HSC cells. (A) Representative immunofluorescence micrographs of fibronectin (FN) in HSC cells on ECM hydrogel substrates subjected to control, TGFβ2 (3 d; 2.5 ng/mL), TGFβ2 + VP (3 d; 0.5 μM). Scale bar, 100 μm. (B) Analysis of fibronectin intensity (N = 30 images per group from 3 HSC cell strains with 3 experimental replicates per HSC cell strain). (C) Representative immunofluorescence micrographs of αSMA in HSC cells on ECM hydrogel substrates subjected to the different treatments. Scale bar, 20 μm. (D) Analysis of percentage of αSMA^{+} cells (N = 3 HSC cells strains, more than 150 cells were analyzed per cell strain). (E and G) Representative

365 fluorescence micrographs of F-actin and p-MLC in HSC cells on ECM hydrogel substrates
366 subjected to the different treatments. Scale bar, 20 µm. (F and H) Analysis of F-actin and p-MLC
367 intensity (N = 30 images from 3 HSC cell strains with 3 experimental replicates per cell strain).
368 Symbols with different colors represent different cell strains. The bars and error bars indicate Mean
369 ± SD. Significance was determined by two-way ANOVA using multiple comparisons tests
370 (*$p<0.05$, ***$p<0.001$, ****$p < 0.0001$).

371

372 ***YAP/TAZ mediate TGFβ2-induced HSC cell contractility***

373 It has been shown that perfusing *ex vivo* human anterior segments with TGFβ2 reduced the
374 length of the SC inner wall [27], suggestive of tissue contraction. HSC cells are known to be highly
375 contractile [3]. To that end, we observed that HSC cell-laden hydrogels were markedly more
376 contractile than comparable HTM cell-encapsulated hydrogels, reaching ~35-42% of their original
377 size by 5 d with normal donor-to-donor variability (**Suppl. Fig.2**). Our data so far showed that
378 YAP/TAZ inhibition reduced pathologic actomyosin cytoskeleton remodeling. Therefore, we
379 hypothesized that TGFβ2 may increase HSC cell contractility, which could be reduced by
380 YAP/TAZ inhibition. To test this hypothesis, we encapsulated HSC cells in ECM hydrogels - a
381 method developed in our laboratory to characterize HTM cell behavior [26, 30, 43] - and treated the
382 constructs with TGFβ2, either alone or in combination with VP, to assess the level of hydrogel
383 contraction at 5 d. TGFβ2-treated HSC hydrogels exhibited significantly greater contraction
384 compared to controls (62.79% of controls; **Fig. 5A,B**), consistent with our previous studies using
385 HTM cells [26, 30, 43]. Co-treatment with VP significantly decreased pathologic HSC hydrogel
386 contraction (81.56% of controls) compared to TGFβ2-treated samples (**Fig. 5A,B**), but it did not
387 fully restore baseline levels. Of note, the influence of VP on HSC cell-laden hydrogel contraction
388 differed between HSC cell strains, showing a stronger effect on HSC02 than HSC03 and HSC09
389 consistent with normal donor-to-donor variability (**Fig. 4A,B**). To rule out that hydrogel
390 contractility was influenced by the cell number, we assessed HSC cell viability in constructs

subjected to the different treatments. No differences were observed for HSC cell-laden hydrogels across groups (**Fig. 5C**).

Together, these data demonstrate that TGFβ2 robustly induces HSC cell contractility in a 3D ECM microenvironment across multiple cell strains, and that pharmacologic YAP/TAZ inhibition potently decreases pathologic HSC cell contraction.

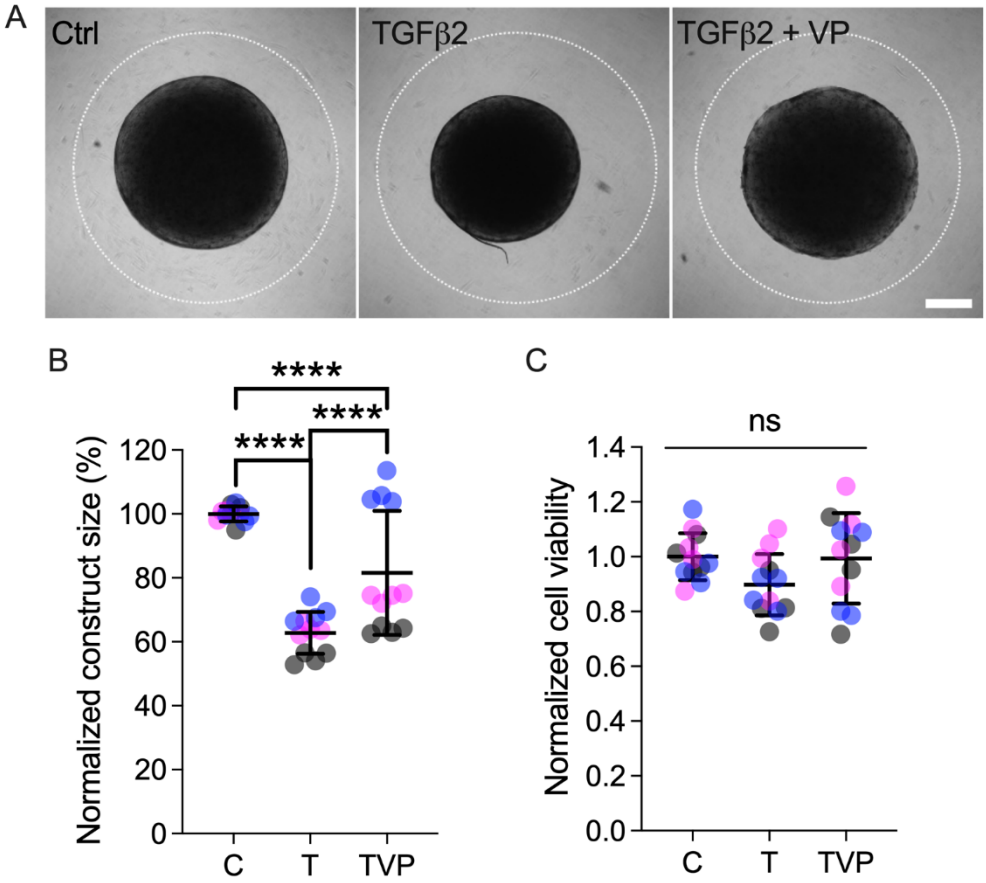

Fig. 5. Effects of TGFβ2 in the absence or presence of YAP/TAZ inhibition on HSC hydrogel contractility. (A) Representative brightfield images of HSC hydrogels subjected to control, TGFβ2 (3 d; 2.5 ng/mL), TGFβ2 + VP (3 d; 0.5 μM) at 5 d (dashed lines outline original size of constructs at 0 d. Scale bar, 1 mm). (B) Construct size quantification of HSC hydrogels subjected to the different treatments at 5 d (N = 12 hydrogels per group from 3 HSC cell strains with 4 experimental replicates per HSC cell strain). (C) Cell viability quantification of HSC hydrogels subjected to the different treatments at 5 d (N = 12 hydrogels per group from 3 HSC cell strains with 4 experimental replicates per HTM cell strain). Symbols with different colors represent different cell strains. The bars and error bars indicate Mean ± SD. Significance was determined by two-way ANOVA using multiple comparisons tests (****$p<0.0001$).

407

408 **Discussion**

409 The profibrotic cytokine TGFβ2 is a key contributor to outflow tissue dysfunction in POAG
410 [10, 19]. TGFβ2 has been shown to increase the deposition of ECM material in the JCT-TM beneath
411 the SC inner wall endothelium and contract the SC [26, 27, 30]. Most *in vitro* studies to date
412 investigating the effects of TGFβ2 on outflow cell dysfunction have focused on TM cells [26, 30, 46].
413 In contrast, the contributions of TGFβ2 to SC cell pathobiology are considerably less well
414 understood. A recent multi-ethnic genome wide meta-analysis identified *YAP1* as a potential
415 genetic risk factor for POAG, implicating that YAP (and perhaps TAZ by association) may play a
416 critical role in glaucoma pathogenesis [40]. We have shown that TGFβ2 upregulates YAP/TAZ
417 activity in HTM cells cultured atop or within ECM hydrogels [26]. Here, our aim was to elucidate
418 mechanisms governing YAP/TAZ modulation in HSC cells in response to TGFβ2 by culturing
419 cells on a tissue-mimetic ECM substrate.

420 Glaucomatous SC cells isolated from POAG eyes exhibit higher levels of F-actin compared to
421 normal cells [15]. Consistent with this observation, we found that TGFβ2 significantly increased F-
422 actin fibers in HSC cells (**Fig. 2B,C**). It has been extensively reported that the glaucoma-associated
423 stressors dexamethasone and TGFβ2 stimulate the formation of cross-linked actin networks
424 (CLANs) in HTM cells [49-52]. Yet, we did not observe TGFβ2-induced CLANs in HSC cells. A
425 number of signaling pathways including Smad, Wnt, ROCK and ERK have been shown to
426 modulate CLAN formation in HTM cells [53]. Further research will be necessary to investigate the
427 specific contribution of these important signaling pathways in HSC cell pathobiology in the
428 context of cytoskeletal homeostasis.

429 The transcriptional coactivators YAP and TAZ play important roles in mechanotransduction
430 and POAG pathogenesis [40, 41]. Recently, we showed that activity of YAP/TAZ is upregulated in
431 HTM cells under diverse simulated glaucomatous conditions [26]. However, the mechanisms
432 underlying YAP/TAZ signaling in HSC cells influenced by TGFβ2 remain to be elucidated. We
433 here demonstrated that TGFβ2 increased YAP/TAZ activity in HSC cells, which was potently
434 attenuated by actin cytoskeleton relaxation using Y27632 or actin depolymerization using Lat B
435 (**Fig. 3**). This suggests that actin integrity is required for YAP/TAZ activation in HSC cells.
436 Moreover, we found that a 30 min treatment of Lat B – necessary to preserve HSC cell viability -
437 was more effective than a 3 d treatment of Y27632 on inducing YAP/TAZ cytoplasmic
438 translocalization. A previous study showed that HTM cells can recover to their initial state after
439 removal of Lat B treatment in a short period of time [54]. It would be worthwhile to further
440 investigate whether Y27632/Lat B-reduced YAP/TAZ activity could be reversed with the
441 treatments withheld.

442 Endothelial-to-mesenchymal transition (EndMT) is a process whereby endothelial cells
443 undergo a series of molecular events, such as increased expression of αSMA, fibronectin,
444 vimentin, and collagen types I and III, that lead to a change in phenotype toward mesenchymal-
445 like cells [55, 56]. TGFβ has been shown to induce EndMT, which can contribute to various fibrotic
446 diseases and cancers [56-59]. In a previous study, it was shown that TGFβ2 stimulated EndMT of
447 HSC cells cultured on top of a synthetic biomaterial; downregulation of endothelial cell markers
448 and upregulation of mesenchymal makers were noted [60]. Consistent with this, we showed that
449 TGFβ2 induced EndMT of HSC cells cultured atop tissue-mimetic ECM hydrogels, as indicated
450 by increased expression of αSMA and fibronectin (**Fig. 2D,E, Fig. 4A-D**). Importantly, we found
451 that TGFβ2-induced EndMT was partially blocked by pharmacologic YAP/TAZ inhibition with

452 VP treatment (**Fig. 4A-D**). Moreover, TAP/TAZ inhibition decreased TGFβ2-induced expression
453 of TGM2 (**Suppl. Fig. 1E,F**), which crosslinks fibronectin and thereby stiffens the ECM [61]. This
454 suggests that YAP/TAZ inhibition may decrease ECM stiffness to improve aqueous humor
455 outflow. Therefore, targeting YAP/TAZ signaling in the SC endothelium to inhibit EndMT is an
456 intriguing strategy for managing ocular hypertension.

457 HSC cells are highly contractile [3]. In fact, we found that HSC cells were even more contractile
458 than HTM cells using our ECM hydrogel system (**Fig. 5A**). Actomyosin, the actin-myosin
459 complex, regulates cell contractility in various cell types [62]. HSC cells in absence of any treatment
460 exhibited qualitatively lower levels of actin fibers compared to HTM cells when cultured atop our
461 ECM hydrogels. Therefore, we speculate that the higher degree of HSC cell contractility could
462 stem from upregulated activity of myosin II, which is responsible for producing contraction force
463 [63]. Myosin II activity is primarily regulated by phosphorylation of MLC; this process is mediated
464 by myosin light chain kinase (MLCK) and myosin phosphatase [64]. Importantly, MLCK inhibition
465 has been shown to decrease IOP in rabbit eyes [65]. Blebbistatin, a pharmacologic inhibitor of myosin
466 II adenosine triphosphatase activity, increases outflow facility via blocking the binding of myosin
467 to actin [66]. Futures studies would be necessary to investigate in greater detail the role of myosin II
468 activity and myosin-actin interactions in HSC cell biology.

469 Consistent with our observation on HTM cells, TGFβ2-treated HSC cells exhibited elevated
470 levels of cell contractility-related molecules (i.e., αSMA, F-actin and p-MLC), which correlated
471 with increased HSC hydrogel contraction. Importantly, this TGFβ2-induced pathologic process
472 was potently attenuated by pharmacologic YAP/TAZ inhibition (**Fig. 4C-H, Fig. 5B-D**). Previous
473 studies showed that outflow resistance is modulated by SC cell stiffness, which is directly

474 correlated with their contractility status [14, 67]. It would be worthwhile to further investigate the
475 effects of YAP/TAZ inhibition on HSC cell stiffness.

476 In conclusion, by culturing HSC cells on tissue-mimetic ECM hydrogels, we demonstrated that
477 TGFβ2 drives actin stress fiber formation to upregulate YAP/TAZ activity, and that YAP/TAZ
478 inhibition reduces HSC cell contractility, which may positively affect cell stiffness and outflow
479 resistance. Our findings provide new evidence for a pathologic role of YAP/TAZ hyperactivation
480 in HSC cell pathobiology in glaucoma, and suggest that pharmacologic YAP/TAZ inhibition has
481 promising potential to improve outflow tissue dysfunction.

482

483 **Disclosure**

484 The authors report no conflicts of interest.

485

486 **Funding**

487 This project was supported in part by National Institutes of Health grants R01EY022359
488 and P30EY005722 (W.D.S.) and K08EY031755 (P.S.G), an American Glaucoma Society Young
489 Clinician Scientist Award (to P.S.G.), a Syracuse University BioInspired Seed Grant (to S.H.),
490 unrestricted grants to SUNY Upstate Medical University Department of Ophthalmology and
491 Visual Sciences from Research to Prevent Blindness (RPB) and from Lions Region 20-Y1, and
492 RPB Career Development Awards (to P.S.G. and S.H.).

493

494

Acknowledgments

We thank Dr. Robert W. Weisenthal and the team at Specialty Surgery Center of Central New York for assistance with corneal rim specimens. We also thank Dr. Nasim Annabi at the University of California – Los Angeles for providing the KCTS-ELP, Dr. Alison Patteson at Syracuse University for rheometer access, and Drs. Audrey M. Bernstein and Mariano S. Viapiano at SUNY Upstate Medical University for imaging support. **Author contributions:** H.L., K.M.P., W.D.S., P.S.G., and S.H. designed all experiments, collected, analyzed, and interpreted the data. K.M.P. and W.D.S. provided the HSC reference cells. H.L. and S.H. wrote the manuscript. All authors commented on and approved the final manuscript. P.S.G. and S.H. conceived and supervised the research. **Data and materials availability:** All data needed to evaluate the conclusions in the paper are present in the paper and/or the Supplementary Materials. Additional data related to this paper may be requested from the authors.

References

1. Ashpole NE, Overby DR, Ethier CR, Stamer WD. Shear stress-triggered nitric oxide release from Schlemm's canal cells. *Investigative ophthalmology & visual science* 2014;55:8067-8076.
2. Dautriche CN, Tian Y, Xie Y, Sharfstein ST. A Closer Look at Schlemm's Canal Cell Physiology: Implications for Biomimetics. *J Funct Biomater* 2015;6:963-985.
3. Stamer WD, Braakman ST, Zhou EH, et al. Biomechanics of Schlemm's canal endothelium and intraocular pressure reduction. *Prog Retin Eye Res* 2015;44:86-98.
4. Ethier CR. The inner wall of Schlemm's canal. *Exp Eye Res* 2002;74:161-172.
5. Stamer WD, Roberts BC, Howell DN, Epstein DL. Isolation, culture, and characterization of endothelial cells from Schlemm's canal. *Invest Ophthalmol Vis Sci* 1998;39:1804-1812.
6. Gong H, Francis AW. Schlemm s Canal and Collector Channels as Therapeutic Targets. 2014.
7. Tamm ER. The trabecular meshwork outflow pathways: structural and functional aspects. *Exp Eye Res* 2009;88:648-655.
8. Tamm ER, Braunger BM, Fuchshofer R. Intraocular Pressure and the Mechanisms Involved in Resistance of the Aqueous Humor Flow in the Trabecular Meshwork Outflow Pathways. *Prog Mol Biol Transl Sci* 2015;134:301-314.

527 9. Brubaker RF. Flow of aqueous humor in humans [The Friedenwald Lecture]. *Invest*
528 *Ophthalmol Vis Sci* 1991;32:3145-3166.
529 10. Quigley HA. Open-angle glaucoma. *N Engl J Med* 1993;328:1097-1106.
530 11. Quigley HA, Broman AT. The number of people with glaucoma worldwide in 2010 and
531 2020. *Br J Ophthalmol* 2006;90:262-267.
532 12. Kwon YH, Fingert JH, Kuehn MH, Alward WL. Primary open-angle glaucoma. *N Engl J*
533 *Med* 2009;360:1113-1124.
534 13. Tham YC, Li X, Wong TY, Quigley HA, Aung T, Cheng CY. Global prevalence of
535 glaucoma and projections of glaucoma burden through 2040: a systematic review and meta-
536 analysis. *Ophthalmology* 2014;121:2081-2090.
537 14. Overby DR, Zhou EH, Vargas-Pinto R, et al. Altered mechanobiology of Schlemm's
538 canal endothelial cells in glaucoma. *Proc Natl Acad Sci U S A* 2014;111:13876-13881.
539 15. Kelly RA, Perkumas KM, Campbell M, et al. Fibrotic Changes to Schlemm's Canal
540 Endothelial Cells in Glaucoma. *Int J Mol Sci* 2021;22.
541 16. Tian YI, Zhang X, Torrejon K, et al. A bioengineering approach to Schlemm's canal-like
542 stem cell differentiation for in vitro glaucoma drug screening. *Acta Biomater* 2020;105:203-213.
543 17. Rao PV, Deng PF, Kumar J, Epstein DL. Modulation of aqueous humor outflow facility
544 by the Rho kinase-specific inhibitor Y-27632. *Invest Ophthalmol Vis Sci* 2001;42:1029-1037.
545 18. Kumar J, Epstein DL. Rho GTPase-mediated cytoskeletal organization in Schlemm's
546 canal cells play a critical role in the regulation of aqueous humor outflow facility. *J Cell*
547 *Biochem* 2011;112:600-606.
548 19. Fuchshofer R, Tamm ER. Modulation of extracellular matrix turnover in the trabecular
549 meshwork. *Experimental Eye Research* 2009;88:683-688.
550 20. Granstein RD, Staszewski R, Knisely TL, et al. Aqueous humor contains transforming
551 growth factor-beta and a small (less than 3500 daltons) inhibitor of thymocyte proliferation. *J*
552 *Immunol* 1990;144:3021-3027.
553 21. Inatani M, Tanihara H, Katsuta H, Honjo M, Kido N, Honda Y. Transforming growth
554 factor-beta 2 levels in aqueous humor of glaucomatous eyes. *Graefes Arch Clin Exp Ophthalmol*
555 2001;239:109-113.
556 22. Agarwal P, Daher AM, Agarwal R. Aqueous humor TGF-β2 levels in patients with open-
557 angle glaucoma: A meta-analysis. *Molecular vision* 2015;21:612-620.
558 23. Kasetti RB, Maddineni P, Patel PD, Searby C, Sheffield VC, Zode GS. Transforming
559 growth factor β2 (TGFβ2) signaling plays a key role in glucocorticoid-induced ocular
560 hypertension. *J Biol Chem* 2018;293:9854-9868.
561 24. Ochiai Y, Ochiai H. Higher concentration of transforming growth factor-beta in aqueous
562 humor of glaucomatous eyes and diabetic eyes. *Jpn J Ophthalmol* 2002;46:249-253.
563 25. Picht G, Welge-Luessen U, Grehn F, Lutjen-Drecoll E. Transforming growth factor beta
564 2 levels in the aqueous humor in different types of glaucoma and the relation to filtering bleb
565 development. *Graefes Arch Clin Exp Ophthalmol* 2001;239:199-207.
566 26. Li H, Raghunathan V, Stamer WD, Ganapathy PS, Herberg S. Extracellular Matrix
567 Stiffness and TGFβ2 Regulate YAP/TAZ Activity in Human Trabecular Meshwork Cells.
568 *Frontiers in Cell and Developmental Biology* 2022;10.
569 27. Gottanka J, Chan D, Eichhorn M, Lutjen-Drecoll E, Ethier CR. Effects of TGF-beta2 in
570 perfused human eyes. *Invest Ophthalmol Vis Sci* 2004;45:153-158.

571 28. Han H, Wecker T, Grehn F, Schlunck G. Elasticity-Dependent Modulation of TGF-β
572 Responses in Human Trabecular Meshwork Cells. *Investigative Ophthalmology & Visual*
573 *Science* 2011;52:2889-2896.
574 29. Pattabiraman PP, Rao PV. Mechanistic basis of Rho GTPase-induced extracellular matrix
575 synthesis in trabecular meshwork cells. *Am J Physiol Cell Physiol* 2010;298:C749-763.
576 30. Li H, Henty-Ridilla JL, Bernstein AM, Ganapathy PS, Herberg S. TGFβ2 regulates
577 human trabecular meshwork cell contractility via ERK and ROCK pathways with distinct
578 signaling crosstalk dependent on the culture substrate. *Current Eye Research* 2022;1-41.
579 31. Fuchshofer R, Welge-Lussen U, Lütjen-Drecoll E. The effect of TGF-beta2 on human
580 trabecular meshwork extracellular proteolytic system. *Exp Eye Res* 2003;77:757-765.
581 32. Fuchshofer R, Tamm ER. The role of TGF-β in the pathogenesis of primary open-angle
582 glaucoma. *Cell Tissue Res* 2012;347:279-290.
583 33. Welge-Lüßen U, May CA, Lütjen-Drecoll E. Induction of Tissue Transglutaminase in the
584 Trabecular Meshwork by TGF-β1 and TGF-β2. *Investigative Ophthalmology & Visual Science*
585 2000;41:2229-2238.
586 34. Moroishi T, Hansen CG, Guan K-L. The emerging roles of YAP and TAZ in cancer.
587 *Nature Reviews Cancer* 2015;15:73-79.
588 35. Plouffe SW, Hong AW, Guan K-L. Disease implications of the Hippo/YAP pathway.
589 *Trends in Molecular Medicine* 2015;21:212-222.
590 36. Polansky JR, Fauss DJ, Zimmerman CC. Regulation of TIGR/MYOC gene expression in
591 human trabecular meshwork cells. *Eye (Lond)* 2000;14 (Pt 3B):503-514.
592 37. Zhao B, Wei X, Li W, et al. Inactivation of YAP oncoprotein by the Hippo pathway is
593 involved in cell contact inhibition and tissue growth control. *Genes Dev* 2007;21:2747-2761.
594 38. Silver JS, Günay KA, Cutler AA, et al. Injury-mediated stiffening persistently activates
595 muscle stem cells through YAP and TAZ mechanotransduction. *Sci Adv* 2021;7.
596 39. Low BC, Pan CQ, Shivashankar GV, Bershadsky A, Sudol M, Sheetz M. YAP/TAZ as
597 mechanosensors and mechanotransducers in regulating organ size and tumor growth. *FEBS Lett*
598 2014;588:2663-2670.
599 40. Gharahkhani P, Jorgenson E, Hysi P, et al. Genome-wide meta-analysis identifies 127
600 open-angle glaucoma loci with consistent effect across ancestries. *Nat Commun* 2021;12:1258.
601 41. Dupont S, Morsut L, Aragona M, et al. Role of YAP/TAZ in mechanotransduction.
602 *Nature* 2011;474:179-183.
603 42. Boopathy GTK, Hong W. Role of Hippo Pathway-YAP/TAZ Signaling in Angiogenesis.
604 *Frontiers in Cell and Developmental Biology* 2019;7.
605 43. Li H, Bagué T, Kirschner A, et al. A tissue-engineered human trabecular meshwork
606 hydrogel for advanced glaucoma disease modeling. *Exp Eye Res* 2021;205:108472.
607 44. Perkumas KM, Stamer WD. Protein markers and differentiation in culture for Schlemm's
608 canal endothelial cells. *Exp Eye Res* 2012;96:82-87.
609 45. Keller KE, Bhattacharya SK, Borras T, et al. Consensus recommendations for trabecular
610 meshwork cell isolation, characterization and culture. *Exp Eye Res* 2018;171:164-173.
611 46. Torrejon KY, Papke EL, Halman JR, et al. TGFβ2-induced outflow alterations in a
612 bioengineered trabecular meshwork are offset by a rho-associated kinase inhibitor. *Sci Rep*
613 2016;6:38319.
614 47. Das A, Fischer RS, Pan D, Waterman CM. YAP Nuclear Localization in the Absence of
615 Cell-Cell Contact Is Mediated by a Filamentous Actin-dependent, Myosin II- and Phospho-YAP-

616 independent Pathway during Extracellular Matrix Mechanosensing*. *Journal of Biological*
617 *Chemistry* 2016;291:6096-6110.
618 48. Liu-Chittenden Y, Huang B, Shim JS, et al. Genetic and pharmacological disruption of
619 the TEAD-YAP complex suppresses the oncogenic activity of YAP. *Genes Dev* 2012;26:1300-
620 1305.
621 49. Montecchi-Palmer M, Bermudez JY, Webber HC, Patel GC, Clark AF, Mao W. TGFβ2
622 Induces the Formation of Cross-Linked Actin Networks (CLANs) in Human Trabecular
623 Meshwork Cells Through the Smad and Non-Smad Dependent Pathways. *Investigative*
624 *ophthalmology & visual science* 2017;58:1288-1295.
625 50. Clark AF, Brotchie D, Read AT, et al. Dexamethasone alters F-actin architecture and
626 promotes cross-linked actin network formation in human trabecular meshwork tissue. *Cell Motil*
627 *Cytoskeleton* 2005;60:83-95.
628 51. Yuan Y, Call MK, Yuan Y, et al. Dexamethasone Induces Cross-Linked Actin Networks
629 in Trabecular Meshwork Cells Through Noncanonical Wnt Signaling. *Investigative*
630 *Ophthalmology & Visual Science* 2013;54:6502-6509.
631 52. Filla MS, Schwinn MK, Nosie AK, Clark RW, Peters DM. Dexamethasone-associated
632 cross-linked actin network formation in human trabecular meshwork cells involves beta3 integrin
633 signaling. *Invest Ophthalmol Vis Sci* 2011;52:2952-2959.
634 53. Zhang YE. Non-Smad pathways in TGF-β signaling. *Cell Research* 2009;19:128-139.
635 54. McKee CT, Wood JA, Shah NM, et al. The effect of biophysical attributes of the ocular
636 trabecular meshwork associated with glaucoma on the cell response to therapeutic agents.
637 *Biomaterials* 2011;32:2417-2423.
638 55. Choi KJ, Nam J-K, Kim J-H, Choi S-H, Lee Y-J. Endothelial-to-mesenchymal transition
639 in anticancer therapy and normal tissue damage. *Exp Mol Med* 2020;52:781-792.
640 56. Ma J, Sanchez-Duffhues G, Goumans M-J, ten Dijke P. TGF-β-Induced Endothelial to
641 Mesenchymal Transition in Disease and Tissue Engineering. *Frontiers in Cell and*
642 *Developmental Biology* 2020;8.
643 57. Clere N, Renault S, Corre I. Endothelial-to-Mesenchymal Transition in Cancer. *Frontiers*
644 *in Cell and Developmental Biology* 2020;8.
645 58. Zeisberg EM, Potenta SE, Sugimoto H, Zeisberg M, Kalluri R. Fibroblasts in kidney
646 fibrosis emerge via endothelial-to-mesenchymal transition. *J Am Soc Nephrol* 2008;19:2282-
647 2287.
648 59. Pérez L, Muñoz-Durango N, Riedel CA, et al. Endothelial-to-mesenchymal transition:
649 Cytokine-mediated pathways that determine endothelial fibrosis under inflammatory conditions.
650 *Cytokine Growth Factor Rev* 2017;33:41-54.
651 60. Dautriche CN, Szymanski D, Kerr M, et al. A biomimetic Schlemm's canal inner wall: A
652 model to study outflow physiology, glaucoma pathology and high-throughput drug screening.
653 *Biomaterials* 2015;65:86-92.
654 61. Akimov SS, Krylov D, Fleischman LF, Belkin AM. Tissue transglutaminase is an
655 integrin-binding adhesion coreceptor for fibronectin. *The Journal of cell biology* 2000;148:825-
656 838.
657 62. Murrell M, Oakes PW, Lenz M, Gardel ML. Forcing cells into shape: the mechanics of
658 actomyosin contractility. *Nat Rev Mol Cell Biol* 2015;16:486-498.
659 63. Kolega J. The role of myosin II motor activity in distributing myosin asymmetrically and
660 coupling protrusive activity to cell translocation. *Mol Biol Cell* 2006;17:4435-4445.

661 64. Fukata Y, Amano M, Kaibuchi K. Rho-Rho-kinase pathway in smooth muscle
662 contraction and cytoskeletal reorganization of non-muscle cells. *Trends Pharmacol Sci*
663 2001;22:32-39.
664 65. Honjo M, Inatani M, Kido N, et al. A myosin light chain kinase inhibitor, ML-9, lowers
665 the intraocular pressure in rabbit eyes. *Exp Eye Res* 2002;75:135-142.
666 66. Zhang M, Rao PV. Blebbistatin, a Novel Inhibitor of Myosin II ATPase Activity,
667 Increases Aqueous Humor Outflow Facility in Perfused Enucleated Porcine Eyes. *Investigative*
668 *Ophthalmology & Visual Science* 2005;46:4130-4138.
669 67. Zhou EH, Krishnan R, Stamer WD, et al. Mechanical responsiveness of the endothelial
670 cell of Schlemm's canal: scope, variability and its potential role in controlling aqueous humour
671 outflow. *J R Soc Interface* 2012;9:1144-1155.
672